Gold nanostructured membranes to concentrate low molecular weight thiols, a proof of concept study

Margaux Berthou, Arnaud Pallotta, Jordan Beurton, Thomas Chaigneau, Athanassia Athanassiou, Christophe Marcic, Eric Marchioni, Ariane Boudier, Igor Clarot

Version of Record: https://www.sciencedirect.com/science/article/pii/S1570023222001489
Manuscript_2224901f835d889eff3e0edcd19e7149

Gold nanostructured membranes to concentrate low molecular weight thiols, a proof of concept study

Margaux Berthou[1], Arnaud Pallotta[1,2], Jordan Beurton[1], Thomas Chaigneau[1], Athanassia Athanassiou[3], Christophe Marcic[4], Eric Marchioni[4], Ariane Boudier[1,2] and Igor Clarot[1,2*]

1 Université de Lorraine, CITHEFOR, F-54000 Nancy, France

2 Nanocontrol, F-54000 Nancy, France

3 Smart Materials, Istituto Italiano di Tecnologia, via Morego 30, 16163 Genova, Italy

4 Université de Strasbourg, CNRS, IPHC UMR 7178, F-67000 Strasbourg, France

Abstract

Thiols are very important molecules in the biomedical field involved for example in redox homeostasis. Their detection and quantification remain difficult due to their poor stability (oxidation) linked to their strong reactivity towards other thiols (by the formation of S-S bonds) or other interfering molecules in the medium. Cellulose membranes with immobilized gold nanoparticles (AuNPs) were developed to capture and quantify thiols in simple and complex matrices. This device was first optimized and characterized in terms of nanostructuration and thiol adsorption. *N*-Acetylcysteine (NAC) and reduced glutathione (GSH), chosen as model molecules, were filtered through the device demonstrating a maximal adsorption capacity of 270 and 60 nmol respectively. In a second step, the adsorbed species were subjected to ligand exchange using a more reactive thiol, dithiothreitol. The results showed release rates of approximately 90% for NAC and GSH. Finally, the amount of endogenous GSH in rat plasma was determined without any pretreatment. For the first time to our knowledge, a nanostructured device for the capture, selective and sensitive quantification of thiols is proposed. This device is easy to handle and overcomes matrix effects. Moreover, the very large concentration factor induced by this technology will be a valuable asset to decrease the quantification limits of analytical methods.

Keywords: Gold nanoparticles; Nanostructuration; Thiols quantification; Biological matrix; Extraction device.

1. Introduction

Molecules bearing thiol groups are very usual compounds in biologicals matrices. Biologicals fluids contains many aminothiols such as glutathione, cysteine and homocysteine being the most common. These are molecules well known to limit the production of free radicals such as reactive nitrogen / oxygen species. They also can act as antioxidant thanks to their -SH group. One of the major endogenous low molecular weight thiols with recognized antioxidant properties in human body is glutathione (GSH). In blood it is mainly present in its reduced form (GSH) compared to the oxidized form (GSSG). In tissues, GSH maintains intracellular redox activities and is a key biomarker of different diseases such as cancer or blood pathologies [1]. Analyzed physiological concentrations of GSH in blood and plasma is highly variable. Levels ranging from 100 µM to 10 mM and from 0.6 µM to 100 µM, respectively for blood and plasma, have been reported [1,2]. Considering the importance of such a molecule, several analytical methods were developed to analyze thiols and more particularly GSH. One of the first to be developed was the Ellman's Method [3]. It is a simple spectrophotometric quantification implying the reaction of thiols with 5,5'-dithiobis-(2-nitrobenzoic acid) leading to the formation of 2-nitro-5-thiobenzoate detected at 412 nm in simple matrices (water, buffers …). However, this method does not allow to identify and differentiate different thiols mixed in a sample and its high limit of quantification (LOQ around 3 µM) may be also an issue when compared to the plasma concentrations mentioned above. Finally, this method is not applicable for thiols in complex samples due to matrices effects [4,5].

Numerous methods were developed to overcome this problem [6–8]. GSH have been analyzed in different matrices using non-separative methods such as spectrophotometry, spectrofluorimetry or amperometry [9–11]. These direct methods are simple but have major drawbacks such as their lack of specificity and selectivity. Separative methods were developed to separate GSH from other thiols in complex matrices. High-performance liquid chromatography [12] and capillary electrophoresis [13,14] coupled to UV-Vis spectrophotometry or fluorimetry are the most used separative techniques for biological thiol quantifications. Even if these methods allow to reach interesting limit of quantifications (5 pM for GSH [12]), they present also other drawbacks. Indeed, they often use harmful chemicals and toxic solvents, require several pre-treatment steps or are difficult to implement as they often use derivatized molecules [7,13] to increase separation selectivity or detection sensitivity.

Gold nanoparticles (AuNP) are widely used in various fields, like healthcare as vectors [15] or in biosensors [16–18] for examples. Their current wide use is explained by their remarkable properties. These nanoparticles are biocompatible, easily synthesizable (single-step synthesis without organic solvents [19]) and have very low production costs. One of the numerous interesting properties of AuNP is their capacity to link thiols through their sulfhydryl (SH) functional group. The gold-thiol bond strength is close to a covalent bond (40-50 kcal.mol^{-1}) allowing facilitated linkage with these molecules [20,21] leading to thiol evaluation in various matrices without time-consuming extraction steps. Ghasemi *et al.* [22] have worked on colorimetric sensors based on AuNP aggregation when the particles were in contact with thiols. The major drawback of colloidal AuNP lays in their stability directly linked to physicochemical conditions such as pH and ionic strength, which strongly limit their use in biological samples [23]. Overcoming these limitations can be achieved through the immobilization of the nanoparticles. AuNP can be easily immobilized on supports using several deposition methods such as dip coating [19] or spraying [24]. The immobilization of AuNP on a surface leads to many advantages such as an increase of AuNP stability under physicochemical condition mimicking physiology (salt concentrations, pH, proteins …) or new material properties, antioxidant activity for example [25] . Bubniene *et al.* [26], described the immobilization of AuNP-citrate on mica sheets. In this work, the anchoring of the nanoparticles on the support was ensured by electrostatic interactions with a cationic polymer. The amount of AuNP immobilized per unit area can be easily controlled through the modulation of AuNP concentration in the suspension used to build the device. Material nanostructuration can generate an easy-to-handle device. For example, Markina *et al.* [27] developed a gold nanoparticle-based paper for the evaluation of GSH in human skin. They described a very interesting and simple thiol sensor, but the sensitivity obtained (6.9 µM) was inadequate for plasma evaluation.

The goal of this work was to develop a specific and sensitive nanostructured device for simple adsorption, desorption and quantification of fragile and low concentrated thiols without problematic sample treatment. The principle consisted in the immobilization of highly reactive gold nanoparticles on commercial cellulosic membranes. As a proof of concept, model thiols were analyzed (reduced glutathione (GSH) and *N*-acetylcysteine (NAC)) in a simple matrix. After validation, rat plasma was supplemented and filtered through the nanostructured membrane to study the behavior of the device and test the analytical method with real complex matrices. To the best of our knowledge, this device was the first of its kind and was able to specifically capture, concentrate and quantify low molecular weight thiols without any denaturation pre-analytical step and without use of harmful chemicals or toxic solvents.

2. Experimental section

2.1. Reagents and samples

All reagents and solvents were of analytic grade and used without further purification. KCl was purchased from Carl Roth. Citric acid and KH_2PO_4 were purchased from Labosi. Methanol and Na_2HPO_4 were purchased from Carlo Erba. $K_2S_2O_8$, NaOH 30%, NaCl and HCl 1.0 M were purchased from VWR Chemicals. Phosphate buffer saline solution (PBS) was prepared as follows: [Na_2HPO_4] = 6.68 mM, [KH_2PO_4] = 1.47 mM, [NaCl] = 138.00 mM, and [KCl] = 2.68 mM, the final pH was adjusted to 7.4 with HCl 12 M. Tris-HCl buffer was obtained by dissolving 18.16 g of Tris in 1 L of H_2O, the pH was adjusted to pH = 7.4 with HCl 12 M. Ultrapure deionized water (> 18.2 MΩ cm) was used for the preparation of all solutions. Poly(allylamine hydro-chloride) (PAH) (average molecular weight of 17,500 g.mol^{-1}, pKa = 8.7) was purchased from Sigma Aldrich. Gold chloride salt ($HAuCl_4$), sodium citrate, sodium borohydride, glutathione (GSH), *N*-acetylcysteine (NAC), dithiothreitol (DTT), Sodium Dodecyl Sulfate (SDS), 2-amino-2-hydroxymethyl-1.3-propanediol (Tris), dibroma (Br_2), rhodamine B,

diisopropyl ether, dithio-5,5'-bis(nitro-2-benzoic) acid (DTNB) were from Sigma-Aldrich. Hydrochloric acid, sodium hydroxide, ammonium chloride and sodium chloride were sourced from the VWR chemicals supplier.

For animals and plasma sampling protocol, all experiments were performed in accordance with the European Community guidelines (2010/63/EU) for the use of experimental animals. Male Wistar rats between 280 and 350 g (Charles River, France) were provided by the ACBS (Animalerie Campus Brabois Santé) laboratory animal house. To obtain arterial blood samples, rats were anesthetized (starting 15 min before sample time) with isoflurane (4% in oxygen 2 $L.min^{-1}$). After anticoagulation (500 UI of heparin sodium, intravenous administration), a laparotomy was performed in order to access the abdominal artery. Blood was obtained directly from the artery through a short PTFE catheter (Intraflon 2, Vygon, France) and collected in Vacutainer (Becton Dickinson, USA) tubes containing heparin lithium. Plasma was obtained after centrifugation (10 000 × *g*, 15 min, 4 °C) and keep at −80 °C.

2.2. AuNP synthesis

Citrate stabilized AuNP were synthetized in aqueous solution according to our previous work[28]. Briefly, 1.0 mL of $HAuCl_4$ solution (10 $mg.mL^{-1}$) was added into 90 mL of water and 2.0 mL of 55 mM sodium citrate was added under inert atmosphere (N_2). The solution was stirred for 1 min then 1.0 mL of 19.5 mM $NaBH_4$ was added and the solution was stirred for 10 min under N_2. The resulting 90 ± 3 nM (λ max 514 ± 1 nm) suspension of nanoparticles was stored in the dark at 4°C during a maximum period of 20 days [28]. For all experiments, AuNP with hydrodynamic diameter of 6.5 ± 0.9 nm (core diameter 5.3 ± 1.1 nm) and anionic charge (zeta potential) of -32.6 ± 0.7 mV were used. See Supplementary Information Section S1 for more information on methods used to characterize the synthesized batches used in this study.

2.3. Preparation and characterization of nanostructured membranes

The immobilization supports used were commercial Chromafil cellulosic membranes (CM) (Diameter 25 mm and pore size 0.45 µm). Nanostructurated membrane (NM) construction was realized under pressure and was illustrated in Figure 1.

A first activation step was realized by pushing a 10 $mg.mL^{-1}$ PAH solution in Tris buffer (0.15 M; pH = 7.4) through the membranes for 10 min. Membranes were rinsed for 3 min with Tris solution and nanostructured using AuNP-citrate colloidal suspension (90 nM). A final rinse with Tris was then realized and the last two steps of this process were repeated fifteen times to achieve a high immobilization density (number of AuNP per cm^2 of membrane). Before used, a final rinse with water was realized.

Gold quantification was adapted from a method developed and validated in our laboratory [29] for colloidal AuNP. NM were extracted from the device and cut, then fragments containing AuNP were oxidized with 1.0 mL of a solution of HCl-NaCl-Br_2 (1.000 M – 0.300 M – 0.025 M respectively) during 15 min (stirred at 600 rpm on a Vibramax 100 (Heidolf Instruments)). Four hundred microliters of the suspending solution were then partially evaporated using a Turbovap (Biotage) at 40 °C under inert gas (N_2, 4 psi) for 20 min. 200 µL of NH_4Cl solution (30% m/V), 100 µL of 6 M HCl and 100 µL of Rhodamine B solution (0.084 µM) were added. To extract the ion-pair formed between tetrachloroaurate anion and Rhodamine B, 300 µL of diisopropyl ether was finally added. Tubes were agitated for 3 min at 1500 rpm and centrifuged (Mini Spin Plus, Eppendorf) 3 min at 12100 × *g*. One hundred and fifty microliters of the supernatant (organic phase containing the Au species) were withdrawn, completely evaporated (Turbovap, 5 min, N_2 3 psi) and the dried residue was dissolved in HPLC mobile phase (150 µL) before injection and rhodamine B quantification by HPLC-Visible detection [29]. HPLC analysis were performed on a Shimadzu LC-20 system constituted by the following modules: degasser, quaternary pump (LC 20AD), autosampler (SIL 20AC), Oven and UV-Visible detector (SPD20A). The column and pre-column (Macherey Nagel Nucleosil 100-3 C18, 150/4.6) were thermostated at 40 °C, the mobile phase consisted on a binary mixture of acetonitrile and 0.1% trifluoroactic acid aqueous solution (25/75, V/V). The injection volume was 100 µL. The detector was set at 555 nm and the pump at a flow rate of 1.0 $mL.min^{-1}$.

The surface of nanostructured supports was observed using a Scanning Electron Microscope (SEM) of the FIB (Focused Ion Beam) type and without sample metallization, reference Helios Nanolab 600i and FEI brand. The ion emitting gallium source was set to 20 kV. Infra-red (IR) spectra were acquired using a Fourier Transform Infrared Spectrometer (FTIR) Spectrum Two (Perkin-Elmer) in Attenuated

Total Reflexion mode (ATR). X-ray Photoelectron Spectroscopy (XPS) was performed using an electron spectrometer (Lab2, Specs, Berlin, Germany) equipped with a monochromatic X-ray source (set at 1253 eV) and with a hemispherical energy analyzer (Phoibos, HSA3500, also from Specs). The applied voltage of the Mg Kα X-ray source was set at 12 kV and the applied current at 7 mA. The pressure in the analysis chamber was ≈ 10^{-9} mbar. The large area lens mode was used for both wide and narrow scans. Peakfit V 4.12 was used to fit curves. Parameters were set as follow: smoothing using the Savitsky-Golay equation (1.5%) and linear baseline with two points (3%).

2.4. Thiol Quantification

Thiol quantification was performed by ion-pair reversed phase HPLC or classical Ellman's reaction. For GSH-NAC separation, the HPLC system consisted of a Spectrasystem pump P1000XR equipped with a Spectraseries AS100 injector and coupled to a Gilson UV-VIS-155 detector set at 205 nm. A C18 Thermo Scientific ODS Hypersil column (250/4.6 mm, 5 µm particle diameter) and a Nucleosil EC 4/3 NUCLEODUR C18 HTec precolumn (5 µm) heated at 40 °C was used. The injection volume was 100 µL. The mobile phase consisted of a mixture of octyl sodium sulfate (10^{-3} M, pH 3.0) and acetonitrile (ACN) (97.0/3.0 V/V) with a flow rate of 2.0 mL.min^{-1}. The method was validated as described by ICH Q2(R1) [30], see Supplementary Information Section S2 (Table S1) for more information on validation parameters. For Ellman's reaction, 100 µL of 5,5′-dithio-bis(2-nitrobenzoic) acid solution (1.0 mM) in PBS were added to 500 µL of each sample. This mixture was incubated 10 min at room temperature protected from light then absorbances were read at λ = 412 nm (linearity between 3 and 32 µM).

2.5. Nanostructured device performance evaluation

All RSH solutions (NAC and GSH) were prepared either in PBS buffer (0.148 M; pH = 7.4) or in HPLC mobile phase (octyl sodium sulfate (10^{-3} M, pH 3.0): ACN (97.0:3.0 V/V).

Thiol adsorption. The preliminary study of colloidal AuNP/NAC interactions was performed using solutions obtained by mixing 665 µL gold nanoparticle suspension and 42 µL of 860 µM NAC. These solutions were incubated at room temperature up to 30 min. Samples were centrifuged at 42,000 × *g* for 90 min at 4 °C (Stratos Heraeus Biofuge centrifuge) and remaining thiols were quantified in the supernatant using Ellman's method.

RSH adsorption on NM was performed by filtering 500 µL of RSH solution (from 1.0 to 50.0 µM) on CM (negative control) and NM. The quantification of the remaining free reduced thiols was performed on the filtrate by previously described HPLC method.

For plasma validation, RSH solutions were prepared in phosphate buffer (0.05 M; pH = 2.5) and diluted (1:10) in rat plasma (from 1.0 to 50.0 µM). Then, 500 µL of samples were filtered on CM (negative control) and NM without further purification. The quantification of reduced thiols was performed on the filtrate by previously described HPLC method.

Thiol desorption. Thiols desorption from membranes was realized using dithiothreitol (DTT). Five hundred microliters of 50 mM DTT (corresponding to 25 µmol) were filtered through CM or NM. The quantification of reduced thiols was performed on the filtrate by previously described HPLC method. Desorption protocol was repeated until a complete release of adsorbed molecules was obtained.

3. Results and discussion

3.1. Device Development and characterization.

3.1.1. Nanostructuration optimization

Based on our previous immobilization methodology [25], a nanostructured cellulosic membrane (NM) was developed. A polycation monolayer of polyallylamine hydrochloride (PAH) was first deposited to create a positively charged surface to successively embed the negatively charged AuNP, up to 15 depositions. Immobilized AuNPs were quantified as a function of the number of depositions [29]. Results are shown in Figure 2A. The average quantity of AuNP per cm² of device increased proportionally with the number of depositions. After 15 cycles, the density of AuNP on the membrane was quantified to be 3.6 ± 0.4 × 10^{14} AuNP.cm^{-2}. No saturation was observed during the construction process. Compared to our previously published work, the 3D meshing of the cellulose membrane allowed the immobilization of about 10 times more AuNP compared to the recovery of a glass substrate (3.8 x 10^{13} AuNP.cm^{-2}) [25]. This quantity highlighted the interest of using a cellulosic

membrane as a substrate to maximize AuNP immobilization. As the number of embedded AuNP increased, the specific surface exchange with analytes should increase accordingly.

Images of CM and NM (15 AuNP deposition steps) are shown in Figure 2B and C, respectively. SEM performed on nanostructured filters (Figure 2D) showed the 3D structure formed by the cellulose 0.45 µm pores that constitutes the support. AuNP were also observed on the surface of the membrane (examples with arrows on Figure 2D). The presence of gold was also assessed using SEM coupled with Energy Dispersive X-ray Spectroscopy (EDS). Details of the atomic composition showed the energy signature of gold atoms (Figure 2E) and confirm that AuNP were deposited on the membrane.

The first PAH deposition step was determined to be a key point. The density of immobilized AuNP was found to be at least 5 times lower than NM without polymer deposition ($0.7 \pm 0.2 \times 10^{14}$ AuNP.cm^{-2}) and a high relative standard deviation value (28%) was obtained (n = 3) indicating a problematic lack of reproducibility in nanostructuration. Such results were in accordance with a non-homogeneous coating that could lead to misfunctioning devices or underestimated results.

In addition, as it was previously demonstrated [19], such embedded AuNP showed a huge improvement in their stability and allowed a long-time storage of the device. Gold quantification on newly manufactured devices and after 6 months of storage showed no significant difference, $3.6 \pm 0.4 \times 10^{14}$ AuNP.cm^{-2} versus $3.7 \pm 0.7 \times 10^{14}$ AuNP.cm^{-2} respectively. This gives it the ability to be mass-produced and reduce inter-batch variations.

3.1.2.Device characterization with adsorbed RSH.

NAC and GSH were chosen to evaluate NM specific adsorption capacities as they are widely used and described in the literature [31]. Five hundred microliters of 50 µM of each thiol (corresponding to 25 nmol) were deposited on NM. Device membranes were then analyzed in Fourier-Transform InfraRed spectroscopy (FTIR). The spectrum corresponding to GSH exposed device presented peaks corresponding to transmittance bands form carboxylic acid (3417 cm^{-1}, 1527 cm^{-1}, 1260 cm^{-1}), amine (2935 cm^{-1}) and primary amido (1642 cm^{-1}) groups (Figure 3). These bands corresponded to functional groups present in GSH molecules and were not detected on pure NM. Similarly, NAC coated device spectrum showed peaks corresponding to transmittance bands of carboxylic acid (3436 cm^{-1}, 1723 cm^{-1}, 1261 cm^{-1}), amine (2928 cm^{-1}) and primary amido (1650 cm^{-1}) groups indicating NAC adsorption (Figure 3).

NM were characterized to investigate the presence of adsorbed thiols through Au-S bounding, as it is well known that compounds can also interact with AuNP thanks to other functional groups [32]. Ellman's reagent (DTNB) was filtered through the device. Should NAC or GSH be linked to AuNP thanks to amine or carboxylic acid groups, their free -SH groups would reduce DTNB reagent and the resulting molecule would be then quantified at 412 nm. For each condition, measured absorbance was below LOQ of Ellman's method (3.2 µM). This LOQ corresponded to 1.6 nmol of thiols in 500 µL, meaning that more than 96% of thiols (1.6 of 25 nmol deposited) were adsorbed thanks to their -SH group to AuNP.

Finally, the chemical and electronic structure of NM with adsorbed GSH was further analyzed by XPS. Nanostructurated membranes displayed peaks for C, N and Au. C and N corresponded to cellulose and/or PAH signatures and were therefore non-specific. On the contrary, Au peaks at 84 and 87 meV were specific to metallic gold (redox state: Au_0) (data not shown) and confirmed the immobilization of AuNP on NM. Thiols exposed NM (GSH and/or NAC) showed an XPS peak at 154 meV, corresponding to sulfur atoms (Figure 4A).

Concomitantly, a right shift occurred on Au peaks. Two contributions were found for the two Au binding energy (Au 4f7/2 and Au 4f5/2): Au0 and Au-S (Figure 4B). The Au 4f7/2 component of the peak at lower binding energy (83.9 meV) was attributed to metallic gold (Au_0), the latter Au 4f7/2 binding energy (84.6 meV) can be associated to Au atoms bounded to S atoms. Similar shift was observed for Au4f5/2 with an energy of 87.6 meV for Au_0 and a binding energy for Au-S of 88.4 meV. Those two shifts are representative of a binding between Au and S [33].

All the previous characterization results demonstrated that NM were able to capture thiols and more precisely with the help of Au-S bounds as expected. This innovative nanostructured device has to be now evaluated in terms of practical use and performances (efficiency and loading capacity).

3.2. First approach

To demonstrate the interest of a nanostructured support, preliminary tests have been performed with classical suspensions of colloidal AuNP. As a first approach, the reactivity of a 90 ± 3 nM AuNP suspension was evaluated with NAC, chosen as model thiol, at a known concentration (50 µM in PBS) and at room temperature. After centrifugation (0 to 90 min), remaining thiols in the supernatant were quantified using Ellman's method to estimate the quantity of thiol adsorbed on AuNP. As illustrated in Figure S3A (Supplementary information, section S3), the addition of AuNP in the media, compared with negative controls (no AuNP), lead to a 90% decrease in NAC concentration. This demonstrated the ability of colloidal AuNP to adsorb thiols, which was consistent with our previous results for similar molecules and associated RSNO [34]. Interaction between colloidal AuNP and thiols was found effective for thiol capture but relied on a time-consuming sample treatment (*i.e.* at least 90 min centrifugation). As a first conclusion, the quantification and the identification of adsorbed thiols cannot be considered without further processing samples or using immobilized nanoparticles. The contact time between AuNP and NAC was studied (Figure S3B) and indicated that the incubation time of the thiol species in the nanoparticle suspension does not influence the global thiol adsorption. As illustrated in Figure S3B, an instantaneous capture rate was observed whatever the contact time under study and led to the possibility of direct filtration of thiol solution through a NM.

3.3. Adsorption and desorption performances

A direct filtration (without any pretreatment time) of 500 µL of 50 µM thiols (corresponding to 25 nmol) was realized with the NM. After HPLC quantification of filtrates, NM was demonstrated to capture 90.7 ± 5.4% and 99.5 ± 0.2% of NAC and GSH respectively. To directly quantify adsorbed thiols, a desorption step was imagined. Two different solutions were considered: desorption based on the reduction of Au-S bound with a strong reducing agent ($NaBH_4$) or through RSH ligand exchange using the dithiol DTT. The first solution was rapidly aborted because of very problematic chromatographic interferences. For the second desorption method, DTT was supposed to have a better affinity for AuNP due to its two thiol groups associated with a low molecular weight. In the literature, DTT was demonstrated to bind to AuNP gold core with a bond-energy higher than 100 $kcal.mol^{-1}$ when both its thiol groups were involved in the linking [35]. To compare, classical thiols usually bond to AuNP gold core with an energy of 40 to 50 $kcal.mol^{-1}$ [20,21]. This energy difference allows DTT to preferentially link to AuNP in place of other thiols [35]. The preferential oxidized form of DTT corresponds to the cyclization through an intramolecular S-S bound, limiting the creation of heteromolecular oxidized dithiols (i.e. DTT-SR dimers). This leads DTT to be the best candidate to I) thiol desorption and II) thiol identification, widely described to chemically desorb thiol molecules from AuNP [32].

For desorption, 500 µL of DTT 50 mM (corresponding to 25 µmol) were filtered through the NM containing adsorbed thiols (NAC and GSH as described in the previous step) and the filtrate was analyzed by HPLC. This operation was repeated until complete desorption and results are shown in Figure 5.

NAC and GSH total releases were achieved after 3 and 6 desorption steps, with a release rate of 89.3 ± 11.4% and 92.1 ± 5.1% of adsorbed thiols, respectively. Even if both thiols were totally desorbed from NM, it required twice the number of desorption steps for GSH compared to NAC. Two hypotheses were raised to explain this matter. i) The steric hindrance difference between NAC and GSH avoids DTT to access the AuNP surface when GSH is absorbed. ii) An affinity difference for AuNP between NAC and GSH. This showed that desorption step must be optimized for each adsorbed thiol, in terms of DTT concentration, repetition number, and contact time. As a first step of optimization, a longer contact time of DTT was consider as Tsai *et al.* had demonstrated that maximal thiol desorption could be obtained after a contact time of several hours [35]. However, one-hour contact time led to very similar results as instantaneous deposition of DTT. The second step was to improve DTT concentration, and a 1 step method (500 µL of 50 mM DTT – or 75 µmol) did not achieved the same desorption rate (31.6 ± 3.4% of desorption) as the 3 steps method (3 times 500 µL of 50 mM DTT – or 3 times 25 µmol).

Evaluation of capture capacity of NM of more complex samples was assessed. Binary mixture of the two thiols (500 µL of 50 µM of both NAC and GSH, corresponding to 25 nmol each) were deposited on NM and quantified before and after the last desorption step. Only 59.0 ± 5.0% of NAC and 50.0 ± 5.6% of GSH were adsorbed when both thiols were deposited. GSH structure and molecular weight is supposed to cause a more important steric hindrance that could prevent NAC to bind on AuNP surface as previously mentioned. The total adsorbed quantity was similar compared to a single thiol adsorption and no competition effect was observed between NAC and GSH indicating the device capacity to trap any low molecular weight thiols in a similar pattern.

After desorption, it appeared that NAC and GSH, when mixed, presented a different behavior to DTT exposition. NAC was preferentially desorbed (83.7 ± 10.1%). Surprisingly, more that 50% of GSH remained adsorbed to NM. Molecules with amino or amido functional groups lead to a stronger adsorption of thiols to AuNP [32]. Figure 5 already showed that NAC desorption was facilitated compared to GSH (with 3 times more amino/amido functional groups than NAC). Indeed, only 3 DTT desorption steps (75 µmol) were required to completely desorb NAC compared to 5 steps (125 µmol) for GSH. The presence of amine functional groups appeared to play a key role in desorption compared to adsorption [36]. It is also suggested that there is a chain-length dependence for thiol binding gold. Lateral interactions between thiols are stronger for high molecular weight thiols, making their desorption more difficult [36,37]. This desorption step may be optimized by pH modification. It was shown that pH higher than amine pKa (pKa = 8.75) can modify GSH conformation and decrease its affinity for Au [32]. But in the case of our device, it could also lead to a partial destruction of the nanostructured membrane due to drastic pH conditions (pH > 11), so this option was not investigated in this paper.

The maximum adsorption capacity of NM was evaluated by repeated filtration of RSH solutions. Results are illustrated on Figure 6 and show that the device maximum capacity (the highest quantity of adsorbed thiols) was 270.0 ± 6.5 nmol and 60.7 ± 3.9 nmol of NAC and GSH, respectively. This corresponded to 410 and 90 molecules of respectively NAC and GSH adsorbed for each AuNP on NM, a very interesting result because it is of the same order as the 550 molecules of NAC adsorbed by each AuNP when not immobilized i.e. in colloidal suspension.

It was previously shown that NAC and GSH behaved differently in terms of desorption, but this appeared to be also the case in terms of NM maximal capacity. The maximal GSH capacity was almost four times lower than NAC capacity. This indicated, as previously stated, that the structural difference between NAC and GSH (molecular weight, functional groups, induced steric hindrance…) played a key role in the ability of the device adsorption. It also gave clue to further response of NM for other low molecular weight thiols adsorption. The integrity of the nanostructured membrane was studied by quantifying the gold after the adsorption and desorption steps. The amount of gold found on the membrane as the different steps are completed is constant ($1.5 \pm 0.1 \times 10^{14}$), an amount of the same order of magnitude as that evaluated before use.

These primordial development steps indicate that the device is effective for the capture and specific release of thiols with good yields. Tests with a similar desorption volume (1.5 mL) but with a larger deposition volume (15 mL) show that the adsorption and desorption efficiencies remained unchanged (> 95%) and allowed us to achieve a sample concentration with a factor of 10. The filtered volume can be much larger and allows us to imagine very high concentration factors, potentially beyond 100 000 (work in progress), thus allowing the quantification of thiols in very low concentration without any prior sample treatment.

3.4. Application to biological samples

The device developed in this work was designed to capture low molecular weight thiols in complex matrices with a two-step analytical strategy. As a first proof of concept, rat plasma was chosen as plasma contains multiple compounds and molecules that can interfere with thiols (thiol bearing proteins, amino acids, oxidazing molecules …). When working with plasma samples, a classical deproteinization step is usually required before HPLC injection. Current deproteinization methods usually involve the use of chemical products such as acidic [38] or organic solvents [39] to precipitate and then remove proteins by centrifugation before analysis. The preanalytical steps could interfere with thiol stability considering the high reactivity of SH functional groups. The pretreatments could modify the GSH/GSSG balance and generate an over or underestimation of one of the species. Surprisingly, direct injection of blank plasma filtered through NM did not induce any high-pressure issues due to protein clogging in the HPLC system. The high reactivity of AuNP toward proteins

coupled to the filtration ability of the device led to a direct deproteinization process, decreasing pretreatment time, avoiding dilution steps or medium modification [40,41]. Rat plasma were spiked with thiols at different concentrations and analyzed in HPLC. Up to 84.0 ± 5.9% of NAC and 90.5 ± 4.2% of GSH were adsorbed from spiked plasma (50 µM), see Supporting Information Section S2 for more information on HPLC method validation parameters. Direct RSH quantification after DTT desorption step was performed as previously described in the development part. A maximum release of 69.3 ± 6.1% and 78.0 ± 8.3% was obtained for NAC and GSH, respectively. The desorption rates were slightly lower than the ones calculated in simple matrices as illustrated in Table 1. This showed that thiol adsorption appeared to be independent from experimental conditions compared to desorption which remained challenging.

Finally, the physiological GSH rat plasma concentration was determined using NM. Plasma GSH concentration was calculated *versus* plasma calibration curve to be 10.4 ± 1.0 µM (5.2 ± 0.5 nmol in 500 µL) (Supplementary information, Figure S4). This value was in accordance with the ones described in the literature [1,2] without any preanalytical steps and/or harmful chemicals. In addition, no interfering peaks were visible on chromatograms as only desorbed GSH and DTT were observed. Hence, this device is perfectly adapted for agri-food matrices with very low thiol concentrations ($ng.L^{-1}$). As an example, Lavigne *et al.* [42] described a wine GSH concentration of 20 $\mu g.L^{-1}$. Five hundred milliliters of this wine filtrated through our NM and eluted with 500 µL DTT would lead to a 1000 times concentration ratio with a GSH quantity of 33 nmol. This advantage will allow the direct quantification of low concentration thiols and avoid LOD/LOQ issues.

4. Conclusion

A gold nanostructured membrane was developed for the first time for specific and sensitive thiols quantification. The device was created by coating of gold nanoparticles on a cellulosic membrane, and then characterized through various techniques. The first part of this study was a proof of concept that aimed to demonstrate the capacity of the device to specifically interact with thiol molecules by forming an Au-S bond. This bond energy is nearly covalent and allows a specific adsorption of these molecules. Thiol adsorption was studied with two model thiols: NAC and GSH that are commonly used in literature. The two thiols were successfully adsorbed in a first step and then released from the device, in a second step, by ligand exchange reaction using a dithiol molecule. Characterization of the two steps was achieved by HPLC. This specific pretreatment method allows to specifically concentrate thiols and is designed for biological samples: no matrix effect, thiol preservation, easily handled … The strong bound between gold and thiol also avoid stability issues (through -SH oxidation essentially) occurring with current thiol analytical methods. Furthermore, the volume needed to desorb leads to a potential analyte concentration.

5. Acknowledgments

Authors would like to thank the Faculty of Pharmacy of Nancy and its Plateforme de Mesures Physico-Chimiques for FTIR measurements as well as Dr. François Dupuis for providing the rat plasma.

6. References

[1] A. Meister, Glutathione metabolism and its selective modification., Journal of Biological Chemistry. 263 (1988) 17205–17208.

[2] E.Y. Park, N. Shimura, T. Konishi, Y. Sauchi, S. Wada, W. Aoi, Y. Nakamura, K. Sato, Increase in the Protein-Bound Form of Glutathione in Human Blood after the Oral Administration of Glutathione, J. Agric. Food Chem. 62 (2014) 6183–6189.

[3] G.L. Ellman, Tissue sulfhydryl groups, Archives of Biochemistry and Biophysics. 82 (1959) 70–77.

[4] B. Halliwell, M. Whiteman, Measuring reactive species and oxidative damage in vivo and in cell culture: how should you do it and what do the results mean?, Br J Pharmacol. 142 (2004) 231–255.

[5] D. Giustarini, A. Milzani, I. Dalle-Donne, R. Rossi, Detection of S-nitrosothiols in biological fluids: A comparison among the most widely applied methodologies, Journal of Chromatography B. 851 (2007) 124–139.

[6] W. Zhu, G. Jiang, L. Xu, B. Li, Q. Cai, H. Jiang, X. Zhou, Facile and controllable one-step fabrication of molecularly imprinted polymer membrane by magnetic field directed self-assembly for electrochemical sensing of glutathione, Analytica Chimica Acta. 886 (2015) 37–47.
[7] X. Dai, Z.-F. Du, L.-H. Wang, J.-Y. Miao, B.-X. Zhao, A quick response fluorescent probe based on coumarin and quinone for glutathione and its application in living cells, Analytica Chimica Acta. 922 (2016) 64–70.
[8] C. Xie, D. Zhong, X. Chen, A fragmentation-based method for the differentiation of glutathione conjugates by high-resolution mass spectrometry with electrospray ionization, Analytica Chimica Acta. 788 (2013) 89–98.
[9] N.N. Sazhina, Determination of Antioxidant Activity of Various Bioantioxidants and Their Mixtures by the Amperometric Method, Russ J Bioorg Chem. 43 (2017) 771–775.
[10] N. Fu, H. Wang, M. Li, G. Zheng, H. Zhang, S. Liang, Spectrofluorimetric Determination of Thiols in Biological Samples with a New Fluorescent Probe 3-Maleimidylbenzanthrone, Analytical Letters. 38 (2005) 791–802.
[11] L. Kukoc-Modun, M. Biocic, N. Radić, Determination of penicillamine, tiopronin and glutathione in pharmaceutical formulations by kinetic spectrophotometry, Acta Pharmaceutica. 71 (2021) 619–630.
[12] S. Melnyk, M. Pogribna, I. Pogribny, R.J. Hine, S.J. James, A new HPLC method for the simultaneous determination of oxidized and reduced plasma aminothiols using coulometric electrochemical detection11This work was funded by a grant from the FDA-Office of Women's Health., The Journal of Nutritional Biochemistry. 10 (1999) 490–497.
[13] J. Hodáková, J. Preisler, F. Foret, P. Kubáň, Sensitive determination of glutathione in biological samples by capillary electrophoresis with green (515nm) laser-induced fluorescence detection, Journal of Chromatography A. 1391 (2015) 102–108.
[14] W. Jin, X. Li, N. Gao, Simultaneous Determination of Tryptophan and Glutathione in Individual Rat Hepatocytes by Capillary Zone Electrophoresis with Electrochemical Detection at a Carbon Fiber Bundle−Au/Hg Dual Electrode, Anal. Chem. 75 (2003) 3859–3864.
[15] A. Llevot, D. Astruc, Applications of vectorized gold nanoparticles to the diagnosis and therapy of cancer, Chem. Soc. Rev. 41 (2012) 242–257.
[16] S.M. Taghdisi, N.M. Danesh, P. Lavaee, M. Ramezani, K. Abnous, An aptasensor for selective, sensitive and fast detection of lead(II) based on polyethyleneimine and gold nanoparticles, Environmental Toxicology and Pharmacology. 39 (2015) 1206–1211.
[17] E. Mele, G.C. Anyfantis, D. Fragouli, R. Ruffilli, A. Athanassiou, Localized synthesis of gold nanoparticles in anisotropic alginate structures, RSC Adv. 4 (2014) 20449.
[18] G. Maiorano, E. Mele, M.C. Frassanito, E. Restini, A. Athanassiou, P.P. Pompa, Ultra-efficient, widely tunable gold nanoparticle-based fiducial markers for X-ray imaging, Nanoscale. 8 (2016) 18921–18927.
[19] A. Pallotta, M. Parent, I. Clarot, M. Luo, V. Borr, P. Dan, V. Decot, P. Menu, R. Safar, O. Joubert, P. Leroy, A. Boudier, Blood Compatibility of Multilayered Polyelectrolyte Films Containing Immobilized Gold Nanoparticles, Part. Part. Syst. Charact. 34 (2017) 1600184.
[20] H. Häkkinen, The gold–sulfur interface at the nanoscale, Nature Chem. 4 (2012) 443–455.
[21] J.C. Love, L.A. Estroff, J.K. Kriebel, R.G. Nuzzo, G.M. Whitesides, Self-Assembled Monolayers of Thiolates on Metals as a Form of Nanotechnology, Chem. Rev. 105 (2005) 1103–1170.
[22] F. Ghasemi, M.R. Hormozi-Nezhad, M. Mahmoudi, A colorimetric sensor array for detection and discrimination of biothiols based on aggregation of gold nanoparticles, Analytica Chimica Acta. 882 (2015) 58–67.
[23] N. Khlebtsov, L. Dykman, Biodistribution and toxicity of engineered gold nanoparticles: a review of in vitro and in vivo studies, (2011) 25.
[24] D. Tejero-Martin, C. Bennett, T. Hussain, A review on environmental barrier coatings: History, current state of the art and future developments, Journal of the European Ceramic Society. 41 (2021) 1747–1768.
[25] J. Beurton, I. Clarot, J. Stein, B. Creusot, C. Marcic, E. Marchioni, A. Boudier, Long-lasting and controlled antioxidant property of immobilized gold nanoparticles for intelligent packaging, Colloids and Surfaces B: Biointerfaces. 176 (2019) 439.
[26] U. Bubniene, M. Ocwieja, B. Bugelyte, Z. Adamczyk, M. Nattich-Rak, J. Voronoyic, A. Ramanaviciene, A. Ramanavicius, Deposition of gold nanoparticles on mica modified by poly(allylamine hydrochloride) monolayers, Colloid Surf. A-Physicochem. Eng. Asp. 441 (2014) 204–210.
[27] M. Markina, N. Stozhko, V. Krylov, M. Vidrevich, Kh. Brainina, Nanoparticle-based paper sensor for thiols evaluation in human skin, Talanta. 165 (2017) 563–569.

[28] A. Pallotta, A. Boudier, P. Leroy, I. Clarot, Characterization and stability of gold nanoparticles depending on their surface chemistry: Contribution of capillary zone electrophoresis to a quality control, Journal of Chromatography A. 1461 (2016) 179–184.
[29] A. Pallotta, V. Philippe, A. Boudier, P. Leroy, I. Clarot, Highly sensitive and simple liquid chromatography assay with ion-pairing extraction and visible detection for quantification of gold from nanoparticles, Talanta. 179 (2018) 307–311.
[30] ICH Q2 (R1) Validation of analytical procedures: text and methodology, European Medicines Agency. (1996).
[31] K. Erkkila, S. Kyttanen, L. Dunkel, Y.H. Lue, C. Wang, A.P. Sinha-Hikim, R.S. Swerdloff, N-acetyl-L-cysteine (NAC) restores GSH-GSSG ratio and prevents human male germ cell apoptosis, J. Androl. (2006) 51–51.
[32] D.-H. Tsai, M.P. Shelton, F.W. DelRio, S. Elzey, S. Guha, M.R. Zachariah, V.A. Hackley, Quantifying dithiothreitol displacement of functional ligands from gold nanoparticles, Anal Bioanal Chem. 404 (2012) 3015–3023.
[33] F. Vitale, I. Fratoddi, C. Battocchio, E. Piscopiello, L. Tapfer, M.V. Russo, G. Polzonetti, C. Giannini, Mono- and bi-functional arenethiols as surfactants for gold nanoparticles: synthesis and characterization, Nanoscale Res Lett. 6 (2011) 103.
[34] J. Tournebize, A. Boudier, A. Sapin-Minet, P. Maincent, P. Leroy, R. Schneider, Role of Gold Nanoparticles Capping Density on Stability and Surface Reactivity to Design Drug Delivery Platforms, ACS Appl. Mater. Interfaces. 4 (2012) 5790–5799.
[35] D.-H. Tsai, T.J. Cho, F.W. DelRio, J.M. Gorham, J. Zheng, J. Tan, M.R. Zachariah, V.A. Hackley, Controlled Formation and Characterization of Dithiothreitol-Conjugated Gold Nanoparticle Clusters, Langmuir. 30 (2014) 3397–3405.
[36] L. Kankate, A. Turchanin, A. Gölzhäuser, On the Release of Hydrogen from the S−H groups in the Formation of Self-Assembled Monolayers of Thiols, Langmuir. 25 (2009) 10435–10438.
[37] R.G. Nuzzo, B.R. Zegarski, L.H. Dubois, Fundamental studies of the chemisorption of organosulfur compounds on gold(111). Implications for molecular self-assembly on gold surfaces, J. Am. Chem. Soc. 109 (1987) 733–740.
[38] Y. Wang, Y. Xie, M. Bernier, I.W. Wainer, Determination of free and protein-bound glutathione in HepG2 cells using capillary electrophoresis with laser-induced fluorescence detection, Journal of Chromatography A. 1216 (2009) 3533–3537.
[39] A.F. Loughlin, G.L. Skiles, D.W. Alberts, W.H. Schaefer, An ion exchange liquid chromatography/mass spectrometry method for the determination of reduced and oxidized glutathione and glutathione conjugates in hepatocytes, Journal of Pharmaceutical and Biomedical Analysis. 26 (2001) 131–142.
[40] D. Tsikas, M. Schmidt, A. Böhmer, A.A. Zoerner, F.-M. Gutzki, J. Jordan, UPLC–MS/MS measurement of S-nitrosoglutathione (GSNO) in human plasma solves the S-nitrosothiol concentration enigma, Journal of Chromatography B. 927 (2013) 147–157.
[41] K. Kowalska, M. Zalewska, H. Milnerowicz, The application of capillary electrophoresis in the determination of glutathione in healthy women's blood, J Chromatogr Sci. 53 (2015) 353–359.
[42] V. Lavigne, A. Pons, D. Dubourdieu, Assay of glutathione in must and wines using capillary electrophoresis and laser-induced fluorescence detection: Changes in concentration in dry white wines during alcoholic fermentation and aging, Journal of Chromatography A. 1139 (2007) 130–135.

Figure and Table Captions

Figure 1. Schematic illustration of the membrane nanostructuration process.

Figure 2. Gold nanoparticle quantification and pictures of corresponding nanostructured membranes as a function of the of AuNP deposition (A). Images of a CM (B) and NM after 15 deposition steps (C). SEM realized on NM (D) and corresponding analysis of the atomic composition by Energy Dispersive X-ray Spectroscopy (E).

Figure 3. IR spectra of nanostructurated membrane NM after GSH adsorption (black), after NAC adsorption (dark grey) and CM (light grey).

Figure 4. XPS spectra of NM with GSH adsorbed representing (A) sulfur peak and (B) Au4f peaks.

Figure 5. RSH release study from NM: release percentage of previously adsorbed GSH (dotted line) and NAC (continuous line) as a function of DTT quantity filtered.

Figure 6. Saturation study of the NM with NAC (plain line) and GSH (dotted line).

Table 1. Amount of NAC and GSH (spiked in mobile phase or rat plasma) adsorbed and desorbed from 25 nmol initially deposited on the NM.

Figure 1

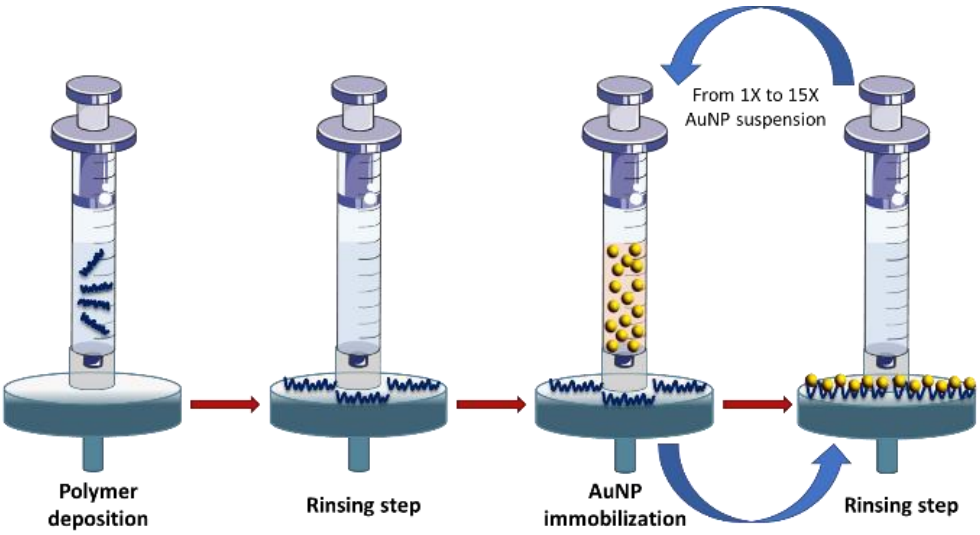
From 1X to 15X
AuNP suspension
Polymer
deposition
Rinsing step
AuNP
immobilization
Rinsing step

Figure 2

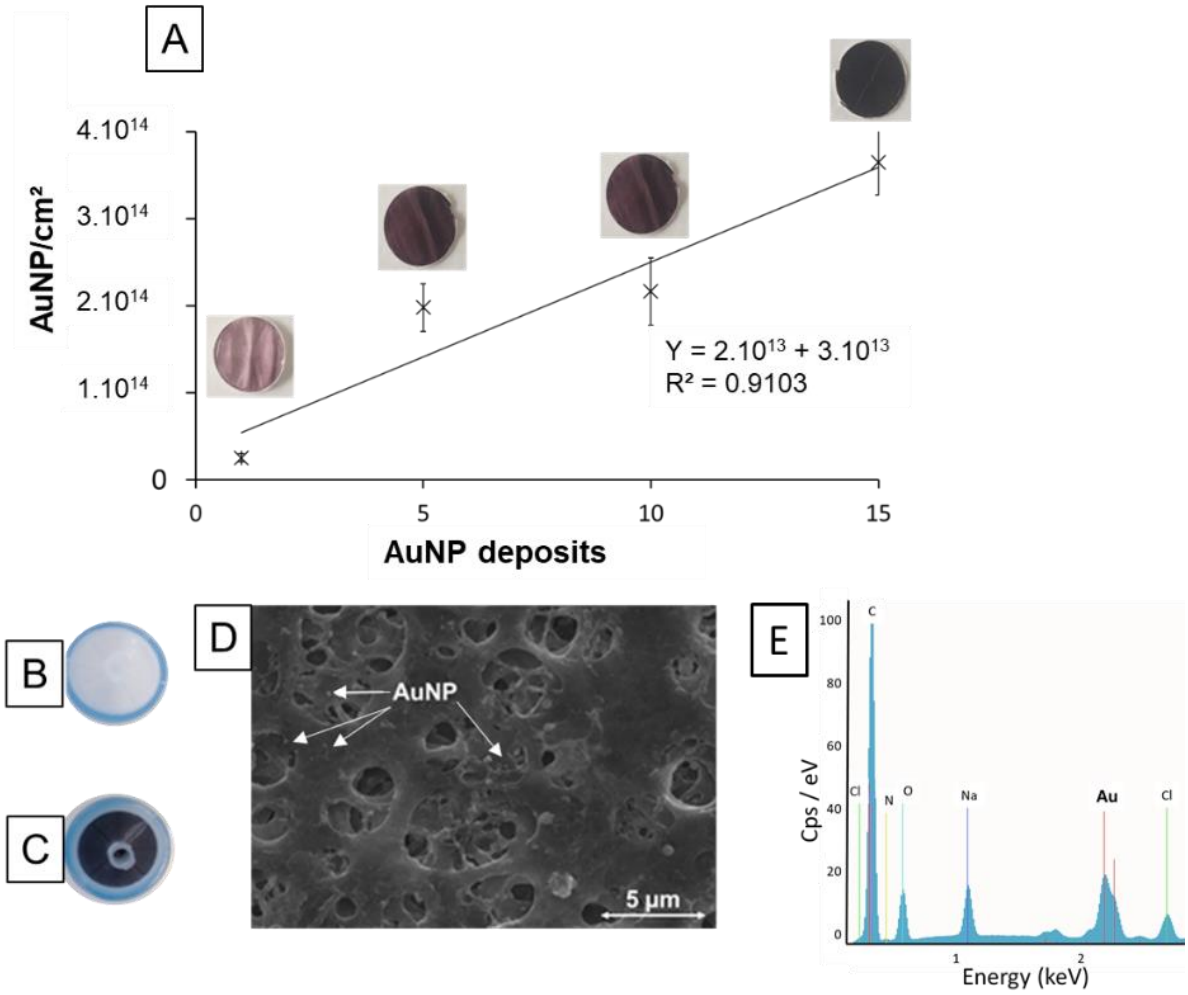
A
AuNP/cm²
4.10¹⁴
3.10¹⁴
2.10¹⁴
1.10¹⁴
0
0
5
10
15
AuNP deposits
Y = 2.10¹³ + 3.10¹³
R² = 0.9103
B
C
D
AuNP
5 µm
E
Cps / eV
100
80
60
40
20
0
C
Cl
N
O
Na
Au
Cl
1
2
Energy (keV)

Figure 3

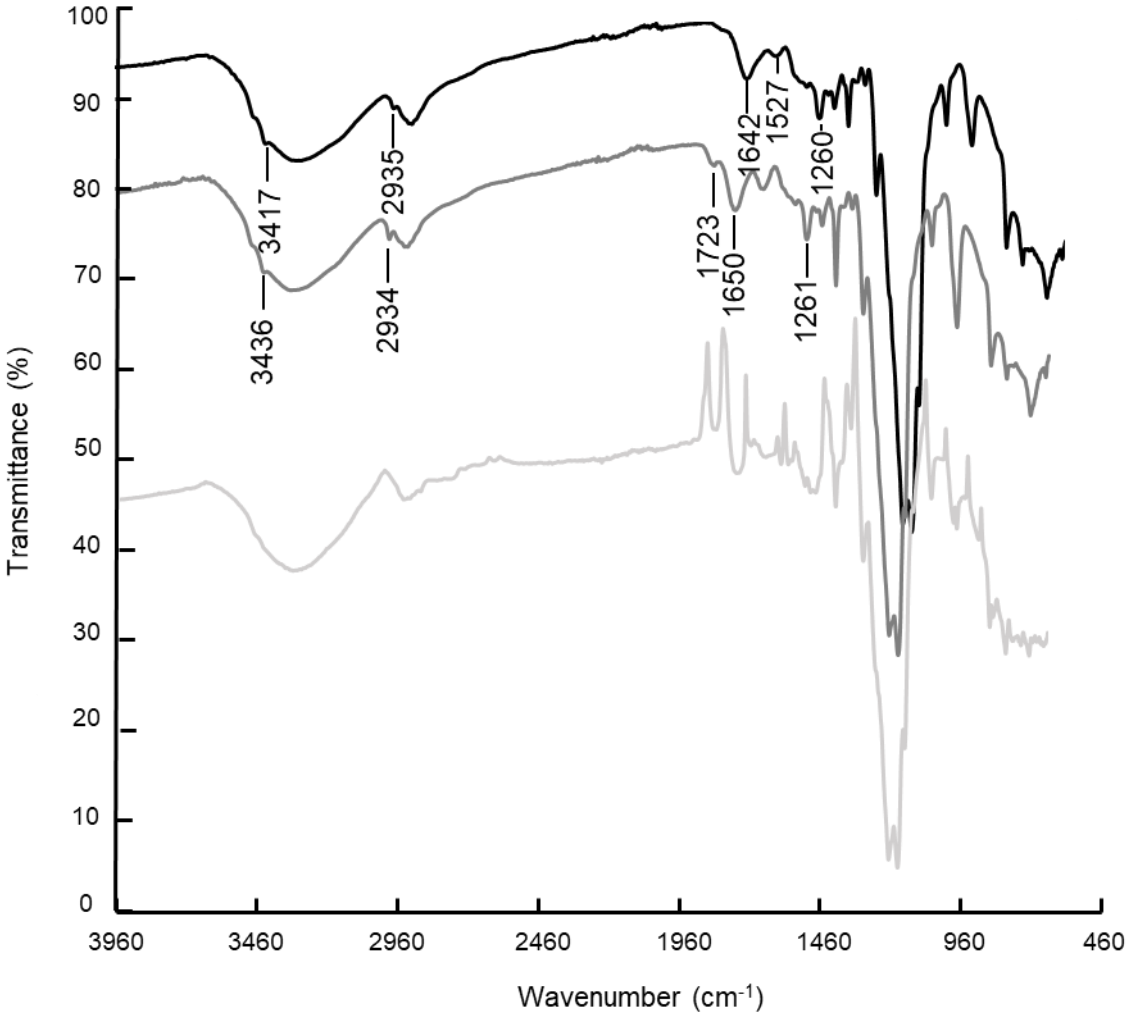
100
90
80
70
60
50
40
30
20
10
0
Transmittance (%)
3960
3460
2960
2460
1960
1460
960
460
Wavenumber (cm-1)
3436
3417
2934
2935
1723
1650
1642
1527
1261
1260

Figure 4

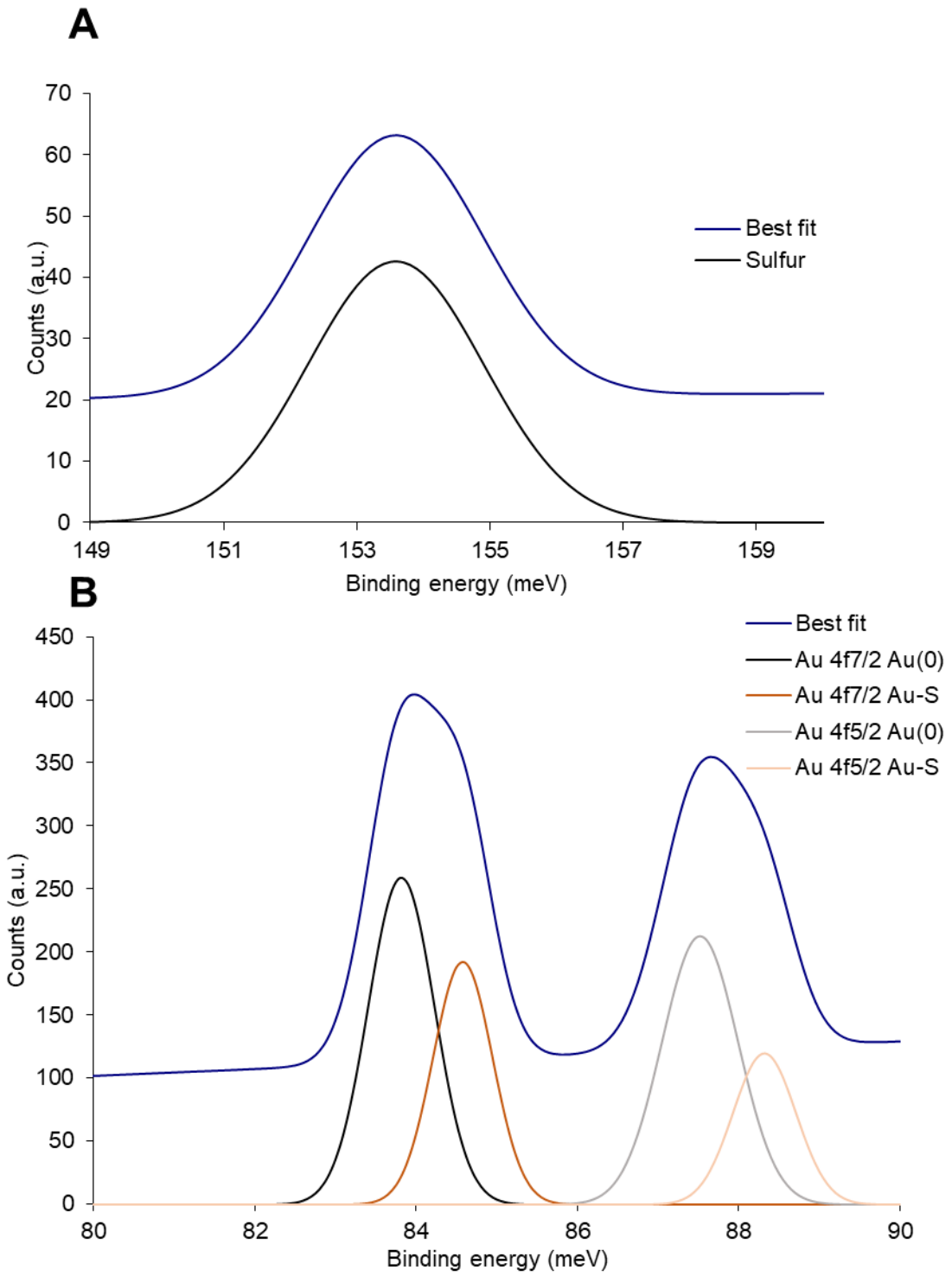
A
70
60
50
40
30
20
10
0
Counts (a.u.)
149
151
153
155
157
159
Binding energy (meV)
Best fit
Sulfur
B
450
400
350
300
250
200
150
100
50
0
Counts (a.u.)
80
82
84
86
88
90
Binding energy (meV)
Best fit
Au 4f7/2 Au(0)
Au 4f7/2 Au-S
Au 4f5/2 Au(0)
Au 4f5/2 Au-S

Figure 5

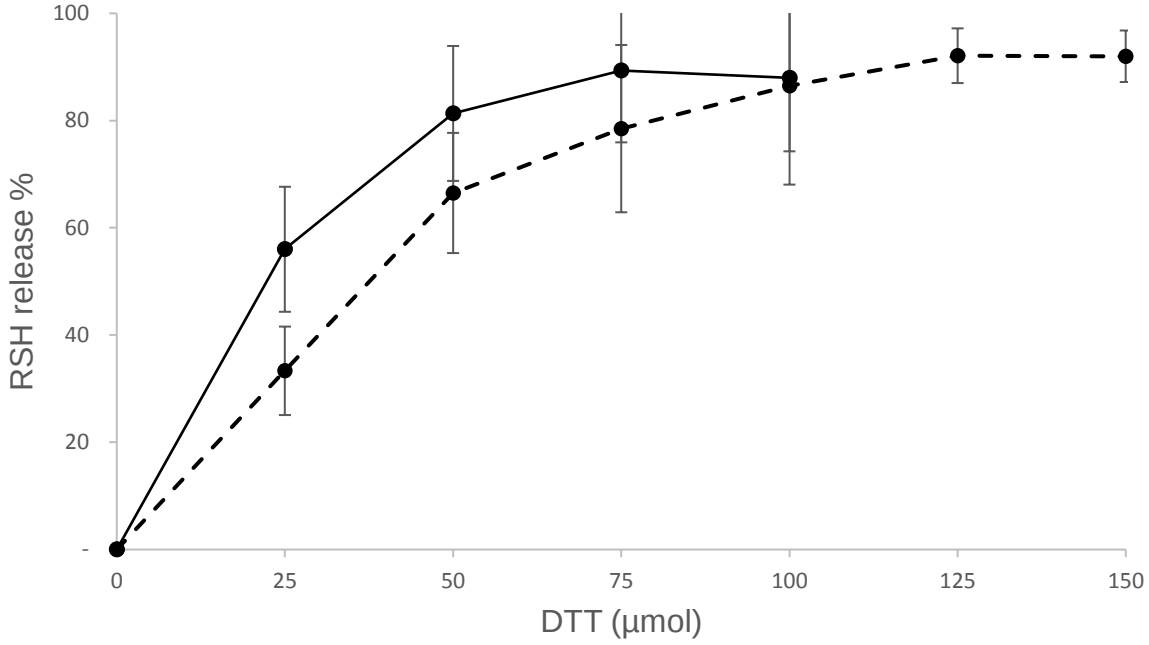

Figure 6

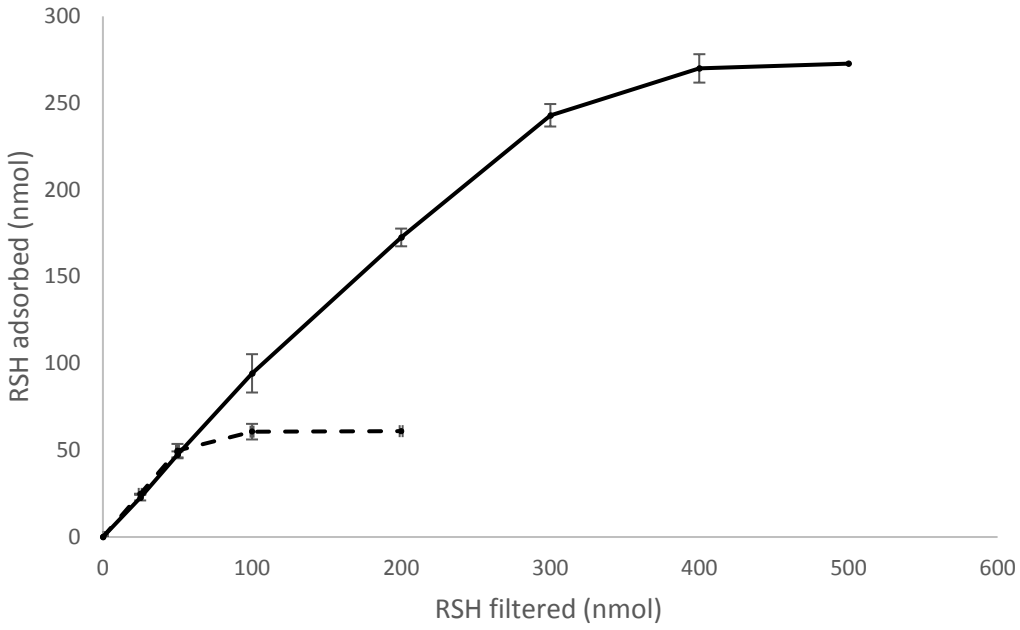
300
250
200
150
100
50
0
RSH adsorbed (nmol)
0
100
200
300
400
500
600
RSH filtered (nmol)

Table 1

		Capture (nmol)	Release (nmol)
NAC	Mobile phase	22.7 ± 1.4	20.0 ± 2.6
	Rat plasma	21.0 ± 1.5	14.6 ± 1.3
GSH	Mobile phase	24.9 ± 0.1	22.9 ± 1.3
	Rat plasma	22.6 ± 1.1	17.6 ± 1.9